

When less is more: TPJ and default network deactivation during encoding predicts working memory performance

Alan Anticevic^{a,*}, Grega Repovs^b, Gordon L. Shulman^c, Deanna M. Barch^d

^a Department of Psychology, Campus Box 1125, Washington University, Saint Louis, MO 63130, USA

^b Department of Psychology, University of Ljubljana, Slovenia

^c Department of Neurology, Washington University in St. Louis, Saint Louis, MO 63130, USA

^d Departments of Psychology, Psychiatry and Radiology, Washington University in St. Louis, Saint Louis, MO 63130, USA

ARTICLE INFO

Article history:

Received 28 July 2009

Revised 29 August 2009

Accepted 4 November 2009

Available online xxx

Keywords:

TPJ

Working memory

Default network

Functional connectivity

ABSTRACT

Previous work has shown that temporo-parietal junction (TPJ), part of a ventral attention network for stimulus-driven reorienting, deactivates during effortful cognitive engagement, along with the default mode network (DMN). TPJ deactivation has been reported both during working memory (WM) and rapid visual search, ostensibly to prevent reorienting to irrelevant objects. We tested whether the magnitude of this deactivation during WM encoding is predictive of subsequent WM performance. Using slow event-related fMRI and a delayed WM task in which distracter stimuli were presented during the maintenance phase, we found that greater TPJ and DMN deactivation during the encoding phase predicted better WM performance. TPJ and DMN, however, also showed several functional dissociations: (1) TPJ exhibited a different task-evoked pattern than DMN, responding to distracters sharing task-relevant features, but not to other types of distracters; and (2) TPJ showed strong functional connectivity with the DMN at encoding but not during distracter presentation. These results provide further evidence for the functional importance of TPJ suppression and indicate that TPJ and DMN deactivation is especially critical during WM trace formation. In addition, the functional connectivity results suggest that TPJ, while not part of the DMN during the resting state, may flexibly “couple” with this network depending on task demands.

© 2009 Published by Elsevier Inc. 37

Introduction

Recent studies have defined two broadly distributed but functionally distinct cortical networks involved in allocation of attentional resources: the dorsal and the ventral attention systems (Corbetta et al., 2002, 2008). One key region of the ventral attention system is the right temporo-parietal junction (TPJ), situated at the intersection of the posterior end of the superior temporal sulcus and the inferior parietal lobule. Previous work has suggested that TPJ is involved in reorienting attention to the external environment when behaviorally important stimuli are encountered (Arrington et al., 2000; Corbetta et al., 2000; Downar et al., 2001; Indovina and Macaluso, 2007; Macaluso et al., 2002; Marois et al., 2000; Serences et al., 2005) and that it is maximally responsive to behavioral relevance of stimuli rather than their sensory salience (Indovina and Macaluso, 2007; Kincade et al., 2005). For instance, previous work showed that TPJ is most responsive when an unexpected environmental stimulus is encountered (Downar et al., 2000, 2001, 2002) that matches the features of the current task (Serences et al., 2005). While reorienting to behaviorally important stimuli is critical for an animal's survival, reorienting to

irrelevant stimuli may interfere with ongoing task performance. Therefore, during effortful cognitive engagement (e.g., encoding novel information into working memory) it may be advantageous to impose an attentional filter that restricts TPJ activation, protecting the ongoing focus of attention from distraction (Shulman et al., 2003, 2007; Todd et al., 2005).

In line with the idea that TPJ deactivation may be necessary at times, previous work has shown that TPJ is deactivated when cognitive demands are imposed (e.g. WM or difficult perceptual search) and the dorsal attention system is engaged (Shulman et al., 2003; Todd et al., 2005). Shulman and colleagues (2003) showed that TPJ was deactivated in a rapid-visual search paradigm (RSVP) prior to target onset when subjects monitored a stream of letters for a target digit, and that the mean magnitude of deactivation was greater on trials in which the subsequent target was detected than on trials in which it was missed (Shulman et al., 2007). They postulated that the magnitude of TPJ deactivation reflected the degree of “filtering” of irrelevant information, which ensured that attentional resources were directed towards task-relevant candidate targets (Shulman et al., 2007). Related results have been reported in the context of working memory (WM) tasks. Todd and colleagues (2005) demonstrated TPJ suppression during delayed WM and that the magnitude of TPJ suppression increased at higher WM loads, leading them to postulate TPJ suppression as a mechanism for protecting the contents of WM.

* Corresponding author. Fax: +1 314 935 8790.

E-mail address: aanticev@artsci.wustl.edu (A. Anticevic).

Because TPJ is responsive to information potentially relevant to the task, it may be particularly important to suppress TPJ activity during WM encoding, when re-orienting might interfere with establishing a novel memory trace. However, previous work on TPJ suppression during WM has not explicitly examined whether the amount of suppression, especially during WM trace formation, is related to behavioral performance, similar to the relationship between suppression and performance that has been observed during rapid visual search (Shulman et al., 2007).

While TPJ is deactivated during certain phases of a task, a well-defined system of regions known as the default mode network (DMN) is deactivated under a broader range of conditions (Buckner et al., 2005; Mazoyer et al., 2001; McKiernan et al., 2003; Raichle et al., 2001; Raichle and Snyder, 2007; Shulman et al., 1997) and shows highly correlated activity in the resting state (Fox et al., 2005; Greicius et al., 2003). Importantly, unlike TPJ, the DMN is not activated by behaviorally relevant stimuli and functional connectivity studies indicate that TPJ is not correlated with the DMN in the resting state (Fox et al., 2005). Because the relationship between TPJ and task-negative/default regions is uncertain, we investigated the degree to which TPJ and DMN regions showed similar properties during WM performance. To our knowledge, only one study has investigated the relationship between the DMN and WM performance (Hampson et al., 2006). However, this study examined across-subject variability in performance as a function of connectivity strength in only two default network nodes and did not test whether DMN deactivation is predictive of WM performance within subjects.

Additionally, while TPJ and DMN regions are not functionally coupled in the resting state (Fox et al., 2005), their activity may be correlated during active WM function. One interesting possibility is that the relationship between TPJ and DMN regions changes as different cognitive demands emerge. Therefore, we explored the relationship between TPJ and the DMN during the encoding and maintenance phases of a WM task.

In summary, the current study addressed three main goals: (1) to examine whether the degree of TPJ deactivation during encoding is predictive of subsequent WM performance; (2) to examine whether there are other regions in which suppression during encoding predicts

subsequent WM performance and whether these regions overlap with the DMN; and (3) to characterize the relationship between TPJ and the DMN across different phases of WM.

Materials and methods

Subjects

21 neurologically intact right-handed, healthy adults (8 male and 13 female, mean age = 24.95) were recruited from the Washington University community by the Psychology Department subject coordinator. All subjects completed and signed an informed consent approved by the Washington University Institutional Review Board and were paid \$25 an hour for their participation.

Materials

Subjects performed a Sternberg-type delayed WM task, which was modeled after the task employed by Dolcos and colleagues (Dolcos et al., 2008; Dolcos and McCarthy, 2006; Sternberg, 1969) (see Fig. 1). The task contained two levels of working memory load (2 or 3 complex geometric shapes) and one of three potential distracter types presented during the maintenance period of the WM task: (1) a task-related geometric shape, which was expected to maximally engage TPJ (Serences et al., 2005); (2) a visually complex neutral image; and (3) an emotional image which was highly distracting and salient, but not task-related. A portion of the trials did not contain distraction (total of 30 blank trials randomized across the experiment, 15 at each WM load), but these trials were not the focus of the current study. Trial types were presented randomly to ensure that subjects had no ability to predict the nature of upcoming distraction and could not resort to a consistent filtering strategy for any of the distracter types. Lastly, we opted for a single instead of multiple distracters to examine whether previously published effects generalize when even less distraction is present.

The memory sets and task-related distracters consisted of complex geometric shapes (Attneave and Arnoult, 1956), which were generated using a Matlab algorithm (Collin and McMullen, 2002).

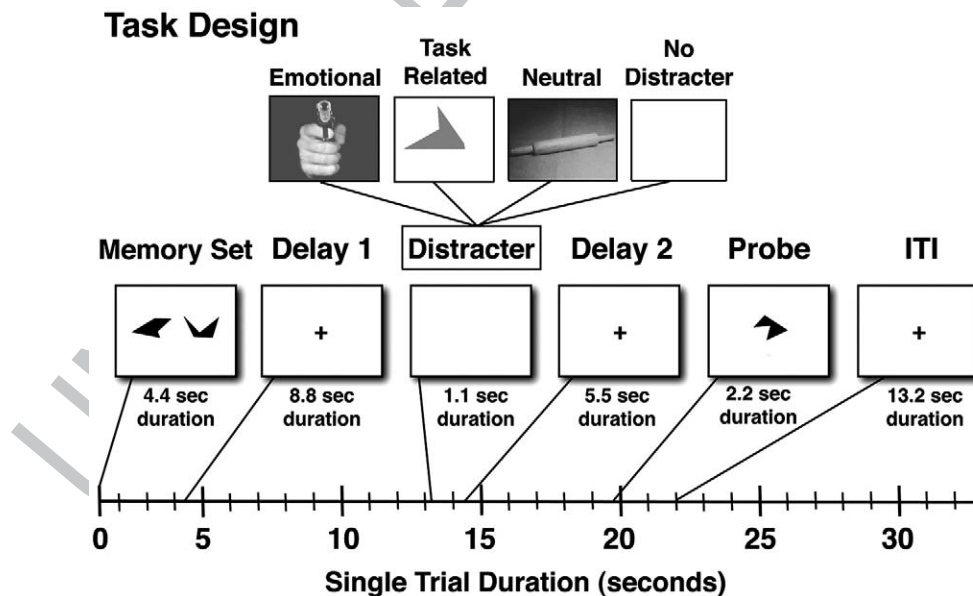


Fig. 1. Task design. A schematic representation of a single trial is shown along with different components and their onsets marked along the timeline. Each box represents a trial component with the duration marked below. First, subjects were presented with a set of complex geometric shapes, which they were instructed to memorize, followed by a delay. Next, during the middle phase of the trial subjects saw either: (1) an emotional distracter; (2) a task-related geometric shape distracter of a different color distinguishing it from the probe; (3) a neutral distracter; or (4) no distraction. This was followed by another delay. Finally, subjects were shown a probe for which they indicated using a button response if it was part of the memorized set or not.

We opted for these stimuli since they were difficult to verbally encode, ensuring maximal modality-specific interference and minimizing subjects' potential use of the articulatory loop for WM maintenance. In other words, we wanted to ensure, as much as possible, that WM trace maintenance is represented in the modality in which distraction was occurring. Also, we wanted to eliminate potential important individual differences in the degree to which subjects can engage verbal maintenance strategies. Memoranda shapes and probes were set to pure black, while task-related distracters were set to a shade of gray to be distinctive from the probes. The emotional and neutral visual distracters were selected from the IAPS stimulus set (Lang et al., 1999) and were equated on luminance, contrast, figure-ground relationships, spatial frequency and color, thus removing previously noted confounds from the stimulus set that may contribute to differences between emotional and neutral stimuli, aside from purely affective properties of the pictures (Bradley et al., 2007; Delplanque et al., 2007; Sabatinelli et al., 2005). All distracters were presented centrally, with a visual angle of 8.5.

Task design

Subjects performed a total of 180 trials, which were divided into 90 high and 90 low WM load trials. There were 25 task-related, 25 emotional, 25 neutral and 15 distracter-free trials in each load condition. The trial sequence was pseudo-randomized with the constraint that no distracter type could appear in more than 3 consecutive trials (to avoid mood induction via emotional distracters). The memory sets were presented centrally with a visual angle of 15.75° for a duration of 4.4 s followed by a 8.8 second delay. The delay was followed by a 1.1 second presentation of the distracter (if present) and then by a 5.5-s post-distracter delay and a probe presented for 2.2 seconds (see Fig. 1). Each trial was followed by a 13.2-s fixation period to allow the hemodynamic response to return to baseline. Prior to the start of the experiment subjects were given instructions explaining the task as well as a brief (8 trial) practice session to demonstrate various trial combinations. The entire experiment was divided into 12 BOLD scanning sequences, each lasting 9.2 min. During the scanning period stimuli were presented through an LCD projector to a screen located behind the scanner, which the subject could see through an angled mirror located above the eyes.

Data acquisition

All subjects were scanned on a 3T Tim TRIO scanner at Mallinckrodt Institute of Radiology at the Washington University Medical School. Functional images were acquired using an asymmetric spin-echo, echo-planar sequence, which was maximally sensitive to blood oxygenation level-dependent (BOLD) contrast (T_2^*) (repetition time [TR] = 2200 ms, echo time [TE] = 27 ms, field of view [FOV] = 256 mm, flip = 90°, voxel size = 4 × 4 × 4 mm). 251 whole-brain volumes were acquired during each BOLD run, each volume consisting of 32 oblique axial slices (4 × 4 × 4 mm resolution) acquired parallel to the anterior-posterior commissure. Structural images were acquired using a sagittal MP-RAGE 3D T1-weighted sequence (TR = 2400 ms, TE = 3.16 ms, flip = 8°; voxel size = 1 × 1 × 1 mm).

Data preprocessing

fMRI data preprocessing steps included: (1) compensation for slice-dependent time shifts; (2) removal of first 5 images from each run during which BOLD signal was allowed to reach steady state; (3) elimination of odd/even slice intensity differences due to interpolated acquisition; (4) realignment of data acquired in each subject within and across runs to compensate for rigid body motion (Ojemann et al., 1997); (5) intensity normalization to a whole-brain mode value of

1,000 but without bias or gain field correction; (6) registration of the 3D structural volume (T1) to the atlas representative template based on 12 normal subjects represented in the Talairach coordinate system (Talairach and Tournoux, 1988) using a 12-parameter affine transform and re-sampled to 1 mm cubic representation (Buckner et al., 2004; Ojemann et al., 1997); (7) co-registration of the 3D fMRI volume to the structural image and transformation to atlas space using a single affine 12-parameter transform that included a re-sampling to a 3-mm cubic representation; and (8) smoothing using a 6 mm full-width at half maximum (FWHM) Gaussian filter.

General fMRI analysis

As a first step a general linear model (GLM) approach was used to estimate magnitudes of task-related activity in each voxel (Worsley and Friston, 1995). We employed an assumed response GLM approach to specifically isolate encoding related activation in addition to other trial components. The model estimated 5 different components of each trial (i.e. encoding, pre-distracter delay, distracter response, post-distracter delay and probe, see Supplemental Fig. S1), obtained by convolving a block function reflecting the neuronal response with a Boynton assumed BOLD response function (Boynton et al., 1996). Distracter response and post-distracter delay were modeled separately for each condition type, whereas encoding and pre-distracter delay components were not, given that subjects had no advance knowledge of upcoming distracter type. All components were modeled separately for both low and high loads. Of note, given the temporal proximity of the distracter and post-distracter delay components we did not make explicit comparisons between the two components and we specifically used the distracter component for the remainder of analyses. An additional assumed response GLM model was computed that included accuracy as a covariate to enable examination of within-subject trial-by-trial relationship between behavioral performance and brain activity. All subsequent statistical analyses used the beta estimates from the assumed response GLM model.

Given the large number of active foci meeting a whole-brain $p < 0.05$ correction in the whole-brain analyses all identified maps were partitioned using a peak-splitting algorithm such that peaks were considered as separate if they were more than 10 mm apart (Kerr et al., 2004; Michelon et al., 2003). In addition, to visualize the activation time courses, we used assumption-free models to estimate signal for each condition (i.e. 2 load levels and 3 distracter-type trials, correct versus incorrect) by estimating 15 time points immediately following trial onset (Boynton et al., 1996). Of note, confirming the validity of our modeling approach, all the results using the assumption-free model analysis did not differ from the ones obtained using an assumption-based model. All whole-brain analyses were visualized using Caret 5.5 software (<http://brainvis.wustl.edu/wiki/index.php/Caret:Download>) and projected on the PALS (population average landmark and surface-based) atlas (Van Essen, 2005).

TPJ ROI identification

To ensure that the TPJ ROI used in the study was defined independently from the current fMRI data, we placed a spherical seed at the center of mass as defined by Shulman et al. (2007) [$x = +52, y = -49, z = +26$] with a radius of 3 functional voxels. This yielded a 123-voxel TPJ ROI, which we used for all reported analyses, and from which we extracted all reported time courses. We opted for the Shulman and colleagues TPJ ROI given that their data were collected at the Imaging Center of the Mallinckrodt Institute of Radiology at the Washington University Medical School, were preprocessed using similar methods and were aligned to the same atlas space (cf. Shulman et al., 2007). In addition, the same a-priori TPJ ROI was used to conduct seed-based connectivity analyses outlined in later sections.

278 *Default network seeds identification*

279 Given that some of the analyses focused on quantitatively verifying
 280 TPJ and DMN activation and connectivity patterns, we employed the
 281 same approach as with TPJ ROI to independently identify all DMN
 282 seeds as defined by Fox and colleagues (2005). Using center of mass
 283 coordinates from Fox and colleagues (2005) we generated spherical
 284 seeds with a radius of 3 voxels for each DMN node. This produced a
 285 total of 13 spherical 123-voxel ROIs, which were used to investigate
 286 TPJ vs. DMN task-evoked signal, ROI-based connectivity computation
 287 and verification of functional connectivity differences at different WM
 288 phases (outlined below).

289 *Functional connectivity preprocessing*

290 Prior to performing functional connectivity (fcMRI) analyses, all
 291 BOLD time series were further preprocessed to remove possible
 292 sources of spurious correlations. All preprocessing, as well as further
 293 fcMRI analyses, were performed using in-house software implemen-
 294 ted in Matlab 7.4 and were based on previously published fcMRI
 295 techniques (Fox et al., 2005). (1) All images were spatially smoothed
 296 using a 6-mm FWHM Gaussian filter (as in the GLM computation
 297 above). (2) To remove low frequencies and scanner drift, images were
 298 temporally filtered using a high-pass filter with a cutoff frequency of
 299 0.009 Hz. (3) Modeled after the procedure employed by Fox and
 300 colleagues (2005) a set of nuisance regressors was removed from the
 301 signal using multiple regression and included: 6 rigid body motion
 302 correction parameters, ventricle signal, deep white matter signal and
 303 whole-brain signal. Whole-brain and ventricle regions were defined
 304 individually for each BOLD run based on its first frame volume using
 305 an automated algorithm. Brain edge was identified using a fixed
 306 threshold. Ventricle centers were identified by peak intensities within
 307 a predefined search volume. Their extent was defined by an iterative
 308 algorithm that searched for large changes in intensity using
 309 previously identified peaks as seeds. Eyes were excluded based on a
 310 predefined mask. As a final step, one layer of boundary voxels was
 311 excluded from both whole-brain and ventricle regions to remove any
 312 possible remaining overlap. All the nuisance regressors were also
 313 expressed as their first temporal derivative to remove their
 314 temporally shifted versions. All subsequent fcMRI analyses were
 315 based on the residual signal after removal was carried out for the
 316 listed nuisance regressors.

317 *Seed-based whole-brain correlation analysis*

318 As described in Introduction, we wanted to investigate the
 319 relationship between TPJ and DMN regions at different phases of
 320 WM to examine whether this relationship changes as the WM process
 321 unfolds. Our first step in addressing this question was to compute and
 322 compare whole-brain seed-based correlation maps at the encoding
 323 and distracter phases of the WM trial using the TPJ ROI as a seed
 324 region (described above). To accomplish this we computed the
 325 average BOLD signal value during the encoding (average of time
 326 points 3 and 4) and distracter phases (average of time points 8 and 9)
 327 at each trial for each voxel in the image. These values were then
 328 concatenated into two 4D (brain volume by trial) series representing
 329 encoding and distracter phase responses over all the trials. TPJ
 330 correlation maps were computed by extracting average values across
 331 all the voxels in the TPJ ROI and computing their correlation with each
 332 voxel in the brain. Importantly, the described approach (i.e. using
 333 isolated time points during each trial and not all the frames in a trial)
 334 effectively enabled us to estimate correlations based on trial-to-trial
 335 variability independent of task structure and avoiding spurious
 336 correlations due to overall task response. Next, encoding and
 337 distracter phase fcMRI maps were computed for each subject
 338 separately. We estimated group-level statistical significance by

converting individual subjects' correlation maps to Fisher Z maps 339
 and computing one-sample *t*-tests for each voxel, comparing the 340
 correlation against zero. Similarly, statistical significance of differ- 341
 ences in fcMRI between different phases of the trial was computed by 342
 performing a paired *t*-test between encoding and distracter phase 343
 Fisher Z values across subjects. All statistical maps were appropriately 344
 corrected for multiple comparisons using cluster size Monte Carlo 345
 algorithms to ensure that the obtained foci met whole-brain false 346
 positive rates of $p < 0.05$. 347

ROI based TPJ-default network analyses 348

The second step in testing the relationship between TPJ and 349
 DMN was to explicitly quantify correlations within DMN ROIs and 350
 between TPJ and DMN ROIs at encoding and distracter phase of the 351
 trial. This was accomplished by extracting mean signal values for 352
 both TPJ and all DMN ROIs in the same manner as described in the 353
 previous section. This enabled us to compute correlations between 354
 all pairs of ROI during encoding and distracter phases separately for 355
 each subject. All the obtained correlations were converted to Fisher 356
 Z values and then entered into a two way: *trial phase* (encoding vs. 357
 distracter phase) \times *connection type* (within-DMN connections vs. 358
 TPJ-to-DMN connections) repeated measures ANOVA. 359

Results 360

Behavioral performance 361

We examined behavioral performance both for the fMRI sample 362
 only ($N = 21$) and by combining the fMRI sample and additional 363
 subjects who completed an identical protocol outside of the scanner 364
 ($N = 19$) for maximal power. Fig. 2 shows the complete profile of 365
 behavioral results. Mean accuracy for the full sample ($N = 40$) was 366
 76.71% for high and 82.65% for low load condition, indicating that the 367
 high load was more behaviorally challenging. To confirm this 368
 statistically we computed a 2-way ANOVA with 4 levels of *condition* 369
 type (task-related, emotional, neutral and distracter-free conditions) 370
 and 2 levels of *load* (high and low). We found a significant *main effect* 371
 of *load* [$F(1,39) = 103.62, p < 0.0001$], a significant *main effect of* 372
distracter type [$F(3,117) = 3.95, p < 0.01$] and a *load by distracter type* 373
interaction [$F(3,117) = 9.17, p < 0.0001$]. The source of the interaction 374
 can be explained by examining the differential effects of distraction at 375
 high versus low load. In the low load: both task-relevant and 376
 emotional distracter conditions were more difficult than the neutral 377
 and distracter-free conditions. However, in the high load condition, 378
 performance did not differ between neutral and emotional distracters, 379
 and task-related distracters were less distracting than either emo- 380
 tional or neutral distracters. 381

Surprisingly, performance in the distracter-free condition under 382
 high WM load was lower than in the distracter conditions. This 383
 pattern of behavioral results was unexpected and may reflect an 384
 artifact of the experimental design. One possibility is that since 385
 distracter trials were much more common than no-distracter trials 386
 and presentation was randomized, subjects may have been 387
 surprised by the probe stimulus on the latter trials, especially 388
 under more difficult conditions (where WM traces may be more 389
 vulnerable). Additional out-of-scanner data from our laboratory 390
 using identical stimuli supports this hypothesis—WM performance 391
 on distracter-free trials was considerably better when they were 392
 presented in a separate initial block than when mixed with all the 393
 distracter trials. Briefly, as shown in Supplemental Fig. S4, when 394
 distracter-free trials were blocked rather than mixed with the rest 395
 of distracter trials, performance was better for distracter-free 396
 conditions at both WM load levels when compared to distracter 397
 trials. This suggests that the distracters used in the present study 398
 did indeed provide some level of interference compared to a non- 399

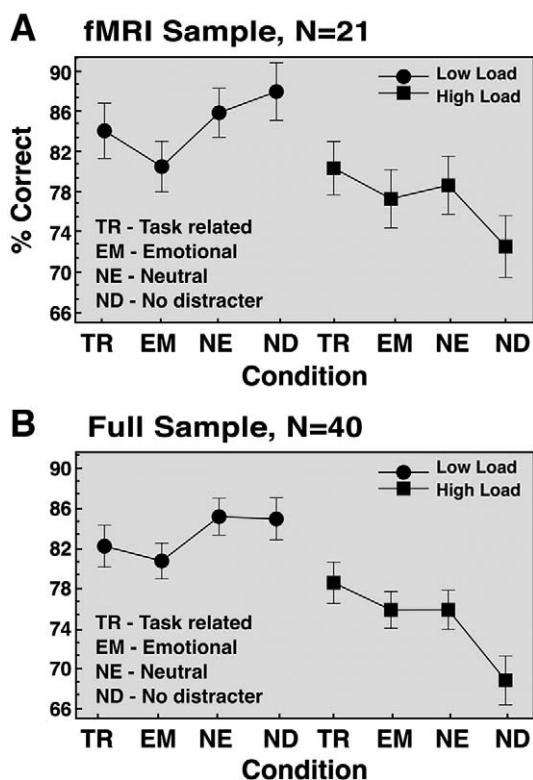


Fig. 2. Behavioral results. Mean accuracy (expressed as % correct) is shown for task-related, emotional, neutral distracter conditions as well as distracter-free trials across two load levels (high load Behavioral results. Mean accuracy (expressed as % correct) is shown for task-related, emotional, neutral distracter conditions as well as distracter-free trials across two load levels (high load = 3 shapes, low load = 2 shapes). Results are shown for the (A) fMRI sample only ($N=21$); and (B) full sample comprised of fMRI and an additional out-of-scanner sample ($N=40$). Both samples received identical versions of the task. Error bars represent ± 1 standard error of the mean.

interleaved distracter-free condition. Nevertheless, the distracter-free condition in the current fMRI sample still fails to accurately represent trials without distraction and for this reason we omitted the distracter-free trials from further fMRI analyses. Below we compare the neural activity for different distracter trials rather than comparing the activity on distracter and distracter-free trials.

Task-evoked TPJ signal

As a first step we sought to replicate previous findings of TPJ suppression during WM (Todd et al., 2005). Figs. 3A–B shows the TPJ ROI and the extracted task-evoked time course averaged across distracter conditions, since our main hypotheses concerned the signal at encoding and participants had no knowledge at that point of the upcoming distracter. TPJ was significantly suppressed during encoding [$t(20) = -3.17, p < 0.005$, two-tailed] (see Fig. 3B) and this deactivation persisted until distracter presentation (dotted vertical line marked by arrow), replicating previous findings (Todd et al., 2005). However, we failed to observe load-dependent TPJ suppression either during encoding [$t(20) = 0.06, p = 0.95$] or pre-distracter delay phases [$t(20) = 0.47, p = 0.64$], possibly due to the difficulty of our WM task (see Discussion).

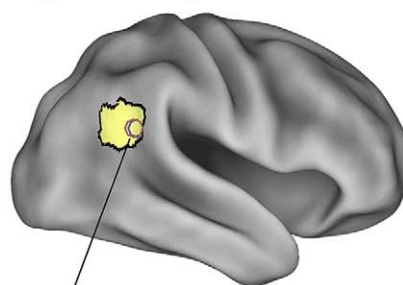
Is TPJ deactivation at encoding predictive of WM performance?

Previous studies have shown that TPJ suppression during visual monitoring, prior to target onset, improves subsequent target detection (Shulman et al., 2007) and others have hypothesized that TPJ suppression may aid WM performance (Todd et al., 2005).

Here we explicitly tested if TPJ suppression at encoding and at different phases of the WM trial predicts behavioral performance.

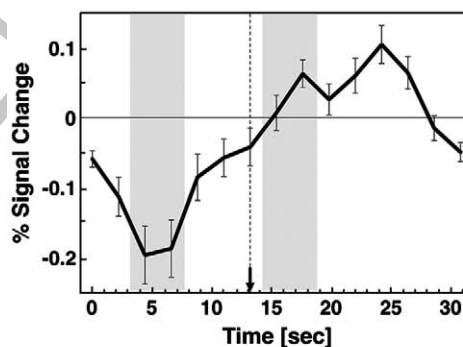
We used a GLM in which correct and incorrect trials were modeled separately (see Materials and methods), allowing us to directly examine—within each subject—differences in BOLD signal magnitude at different phases of the WM process as a function of accuracy. The corresponding TPJ time courses from this analysis for correct (green lines) and incorrect (red dotted lines) trials are shown in Fig. 3C. As before, we collapsed across distracter types, given that at encoding participants had no knowledge of the upcoming distraction. We also averaged across load, given that a similar signal pattern was observed at both load levels. The time courses in Fig. 3C indicated that the TPJ signal was markedly suppressed during encoding and a paired t -test

A Right Hemisphere - TPJ ROI



Todd et al. and Serences et al. ROIs

B Average TPJ Signal



C Correct and Incorrect Trials

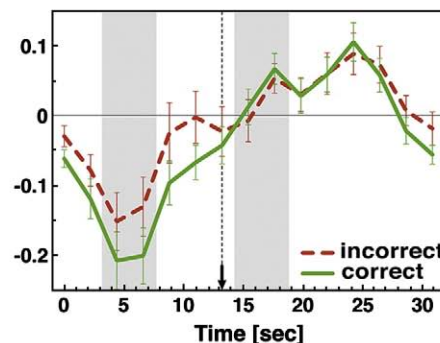
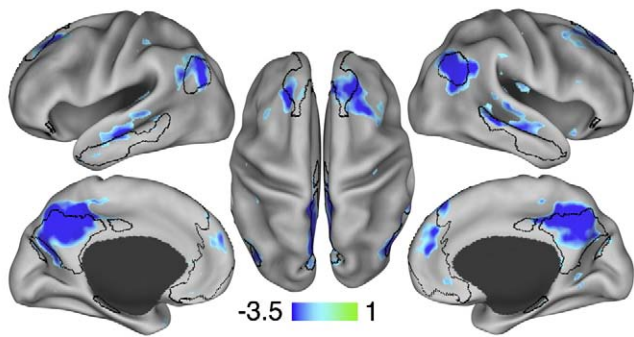


Fig. 3. TPJ time courses. (A) TPJ ROI is shown on the right lateral surface rendering along with foci from previous studies. (B) Average event-related time course is shown for the TPJ ROI averaged across distracter types and loads, given no differences at encoding. (C) Average time course extracted from TPJ ROI is shown for correct (green) and incorrect (red-dotted) trials collapsed across loads and distracter types. Distracter onset is marked by a dotted vertical line ending in an arrow. Encoding and distracter phases are marked with grey bars. Error bars represent ± 1 standard error of the mean. (For interpretation of the references to colour in this figure legend, the reader is referred to the web version of this article.)

A Regions at Encoding: Correct < Incorrect



B Correct and Incorrect Time Courses

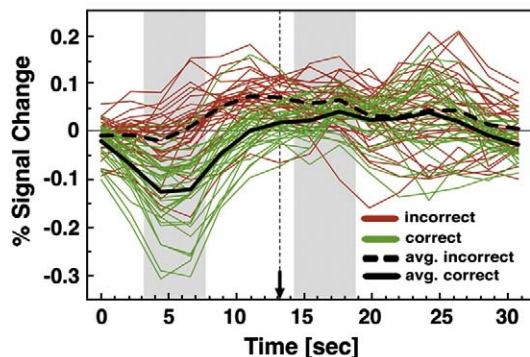


Fig. 4. Other regions showing less signal for correct than incorrect trials during encoding. (A) Regions showing less signal for correct than incorrect trials during the encoding phase closely match the Fox and colleagues (2005) default network regions, which are shown using black border outlines. Here, we show the foci using a $Z > 2.5$ threshold demonstrating that even with a lower cutoff the deactivations are centered mainly around the default network regions and not elsewhere. (B) Average event-related time courses are shown for correct (green) and incorrect (red) trials across all the peak ROIs identified from the map in the top panel after it was corrected for multiple comparisons using cluster size algorithms to ensure whole-brain false positive rates of $p < 0.05$. Each line represents signal for a single ROI averaged across all trial types given no differences between them during encoding. The black lines show the average response across all peak ROIs for correct (solid) and incorrect (dotted) trials. Distracter onset is marked by a dotted vertical line ending in an arrow. Encoding and distracter phases are marked with grey bars. (For interpretation of the references to colour in this figure legend, the reader is referred to the web version of this article.)

indicated that this suppression was significantly greater on correct than incorrect trials [$t(13) = -5.52, p < 0.0001$]. As with the average task-evoked signal, the pattern did not differ across load [$t(13) = 0.36, p = 0.72$]. However, the pre-distracter delay phase component did not show significantly greater suppression on accurate than inaccurate trials [$t(13) = -0.27, p = 0.79$], a result that did not differ as a function of load [$t(13) = 1.29, p = 0.22$]. Finally there were no differences between correct and incorrect trials for the distracter component, as evident in Fig. 3C [$t(13) = -0.25, p = 0.8$]. To confirm that the distracter component did not differ as a function of accuracy, load, or distracter type we computed a 3-way ANOVA with accuracy (correct, incorrect), distracter type (neutral, emotional, task-related) and load (high, low) as factors. No term reached significance. Taken together, these results indicate that greater TPJ suppression specifically during encoding was predictive of better WM performance irrespective of WM load.

Are there other brain regions showing a relationship between deactivation during encoding and WM performance?

We examined if the degree of suppression in any brain region other than the TPJ predicted better WM performance. Beta estimates

during encoding for correct and incorrect trials, averaged over distracter type, were compared using a whole-brain voxel-level t -test, corrected for multiple comparisons ($Z > 3$, cluster size = 13 voxels). This analysis revealed a set of brain regions showing significantly less activation for correct vs. incorrect trials (Fig. 4A) that closely matched the DMN, including bilateral posterior medial, bilateral frontal medial, bilateral superior frontal and bilateral inferior temporal cortical regions, bilateral angular gyrus, and bilateral hippocampal gyrus. We carried out additional analyses confirming that the deactivated foci fell largely within the DMN as defined by Fox and colleagues (2005) (see Supplemental Results). Next we isolated each ROI using a peak-splitting approach (see Supplemental Results) to confirm that the obtained deactivated foci showed the same time course pattern of greater deactivation during encoding for correct than incorrect trials. Fig. 4B shows the signal in DMN foci for correct and incorrect trials collapsed across all conditions (given no differences at encoding across load or distracter condition), and indicates more deactivation at encoding for correct trials. This pattern is also illustrated in Fig. 4B (black lines) averaged across all isolated peaks. We carried out additional analyses to confirm that this pattern was also present for: (1) foci explicitly overlapping the DMN map as defined by Fox and colleagues (2005); and (2) for spherical ROIs defined explicitly using Fox and colleagues (2005) center of mass coordinates (Supplemental Materials and Supplemental Fig. S2A–C). As with TPJ, none of the brain regions showing less signal at encoding for correct vs. incorrect trials showed a similar result at pre-distracter delay or distracter response phases of the WM trial.

Do default regions deactivated during encoding show the same overall signal pattern as TPJ?

Because TPJ and DMN showed very similar task-evoked activation profiles during encoding, we examined whether they showed similar profiles during the distracter and probe phases. We used spherical DMN ROIs defined in the same way as TPJ (see Materials and methods). Foci were combined into a single binary “region” file comprised of all DMN ROIs as defined by Fox and colleagues (2005) to compute the overall response within the DMN. To determine whether this response differed from the TPJ response during the distracter phase, we computed a 3-way ANOVA with distracter type (neutral, emotional, task-related) \times load (hi, low) \times region (TPJ, DMN) as factors. The ANOVA results indicated a significant region \times distracter type interaction [$F(2,40) = 7.87, p < 0.0015$]. The source of the interaction can be seen in Fig. 5, which indicates in line with previous work (Serences et al., 2005) that TPJ was maximally responsive to

Distracter Response - TPJ & DMN

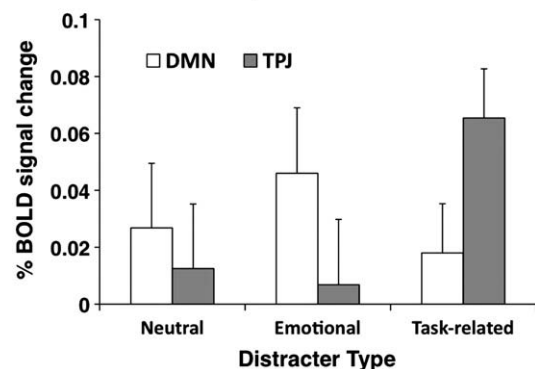


Fig. 5. TPJ and default network distracter response. Magnitudes associated with the distracter response component obtained using the assumed GLM are shown for the TPJ (gray bars) and default network (DMN) (white bars) across different distracter types. Magnitudes are collapsed across loads given no differences as a function of load. Error bars represent ± 1 standard error of the mean.

501 task-related distracters, whereas the DMN showed similar response
 502 magnitudes across the different distracter types. The main effect of
 503 *region* and other terms involving the *region* factor were not significant,
 504 indicating no differences as a function of load and no difference in the
 505 overall distracter response between TPJ and DMN.

506 In addition, we compared TPJ vs. DMN response at the probe
 507 phase. No significant differences were observed between TPJ and
 508 DMN, either overall [$F(1,20) = 1.51, p = 0.23$] or as a function of load
 509 [$F(1,20) = 0.78, p = 0.38$]. However, this lack of difference between
 510 TPJ and DMN at the probe phase appeared to be largely due to the
 511 response of one of the DMN ROI (i.e. retrosplenial cortex), which
 512 showed a substantially more prominent probe response when
 513 compared to other DMN foci (see Supplemental Fig. S2C). Further,
 514 the retrosplenial cortex ROI was not deactivated during encoding,
 515 unlike the other DMN ROIs. Although this ROI was identified as a part
 516 of the DMN in the resting state using a functional connectivity
 517 criterion (Fox et al., 2005, 2006) retrosplenial cortex does not appear
 518 to deactivate along with the rest of the DMN nodes during active
 519 cognitive states (Shulman et al., 1997). When we conducted the above
 520 analysis without the retrosplenial DMN ROI, TPJ showed a signifi-
 521 cantly higher probe response compared to the rest of the DMN [F
 522 (1,20) = 7.43, $p < 0.015$]. Since this exclusion was ad-hoc, however,
 523 the difference in the probe response between TPJ and DMN must be
 524 considered provisional. Overall, these analyses indicate that the task-
 525 induced response pattern in the DMN during the distracter phase and
 526 possibly the probe phase was different than that found in TPJ.

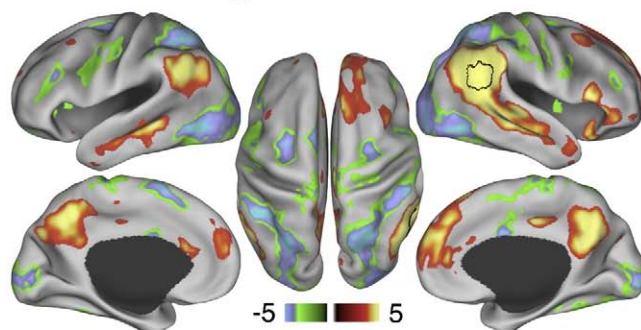
527 *fcMRI analyses of the relationship between TPJ and the DMN*

528 We further examined the relationship between TPJ and DMN
 529 during encoding and distracter phases of the trial using the TPJ ROI as
 530 a seed in trial-based fcMRI analyses. We averaged across all trial types
 531 and load levels at each WM phase separately to gain maximal power.
 532 Fig. 6A shows the pattern of trial-based connectivity between the TPJ
 533 seed and the rest of the brain during encoding (average of time points
 534 3 and 4). Importantly, the use of a single time measurement on each
 535 trial ensured that changes within the trial in task structure did not
 536 contribute to the observed correlation pattern. Regions showing
 537 positive correlations with the TPJ seed at encoding included bilateral
 538 anterior medial and posterior medial cortex, bilateral superior
 539 temporal sulcus, superior frontal cortex and bilateral angular gyrus
 540 (Fig. 6A, red-yellow foci). Conversely, regions showing negative
 541 correlations included bilateral intraparietal sulcus, bilateral region
 542 MT, bilateral insula/frontal operculum, bilateral frontal eye fields and
 543 bilateral SMA (Fig. 6A, blue-green foci). Overall, the positive
 544 correlation map showed strong similarity to the DMN map reported
 545 by Fox and colleagues (2005) (total overlap with Fox et al., 2005 map
 546 was calculated and is shown in Supplemental Fig. S3), while the
 547 negative correlation map showed strong correspondence to the
 548 fronto-parietal task network (Corbetta et al., 2002), as well as other
 549 regions in frontal cortex and insula.

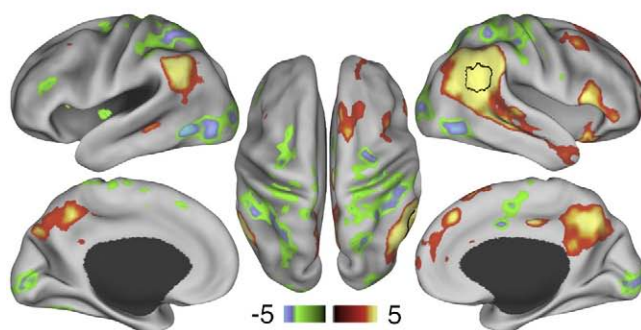
550 Next, we examined whether the pattern of trial-based fcMRI
 551 between the TPJ and the DMN changed as the WM process
 552 unfolded. We carried out the same trial-based fcMRI analysis
 553 during the WM distracter phase (average of time points 8 and 9).
 554 Fig. 6B shows that the pattern of TPJ trial-based connectivity during
 555 distracter phase demonstrated many similarities to the pattern
 556 found during encoding. Nevertheless, functional connectivity during
 557 distracter and encoding phases showed significant differences, as
 558 indicated by a whole-brain paired *t*-test using individual Fisher *Z*
 559 values that compared encoding vs. distracter phase TPJ trial-based
 560 connectivity (Fig. 6C). Fig. 6C indicates that the TPJ showed a
 561 decrease in trial-based correlation with the DMN foci during the
 562 distracter phase as compared to encoding (indicative of “de-
 563 coupling” between TPJ and DMN during distraction), but an
 564 increase in correlations with most regions of the dorsal fronto-

TPJ Seed fcMRI

A Encoding Phase



B Distracter Phase



C Distracter vs. Encoding Phase

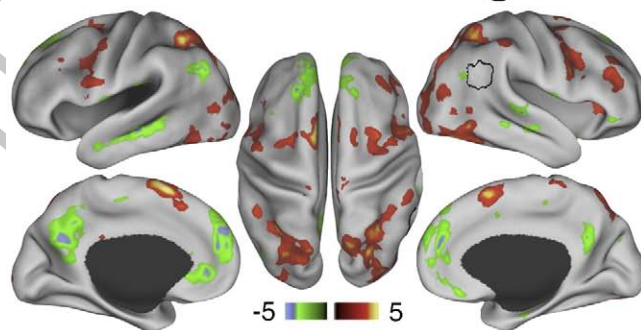


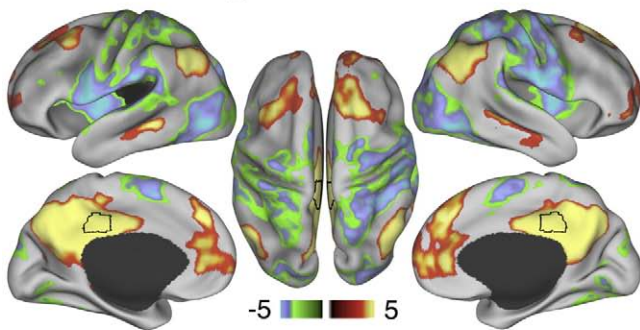
Fig. 6. Relationship between TPJ and default network at encoding and distracter phases. All maps are shown using *Z* statistics. (A) During the encoding phase TPJ seed ROI shows positive correlations (red-yellow colors) with main nodes of the default network and negative correlations (green-blue colors) with main components of the dorsal task network. (B) During the distracter phase the pattern is similar, but attenuated. (C) Maps show results of a paired *t*-test comparing TPJ ROI trial-based connectivity during distracter vs. encoding phase. Red-yellow map shows regions where correlations with the TPJ seed increased from encoding to distracter phase, whereas the green-blue map shows regions where correlations with the TPJ seed decreased from encoding to distracter phase, indicative of “de-coupling.” We show the map at $Z > 2.5$ to illustrate that the TPJ (shown in black border outline) “de-couples” mainly from the default network and not other cortical regions, but ‘couples’ more strongly with the dorsal task network. All peaks shown were present after applying a multiple comparison correction using cluster size algorithms to ensure whole-brain false positive rates of $p < 0.05$. (For interpretation of the references to colour in this figure legend, the reader is referred to the web version of this article.)

565 parietal task network including other frontal regions and anterior
 566 insula. In summary, these results suggest that as the WM process
 567 unfolded, TPJ coupling with the DMN decreased, whereas coupling
 568 with the dorsal attention system increased.

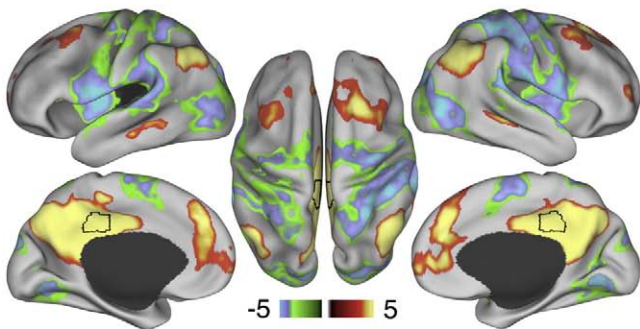
569 The same analysis was conducted using a canonical posterior
 570 medial cortex (precuneus) DMN ROI, which was identified using the
 571 center of mass as defined by Fox and colleagues (2005) and was the
 572 same size as TPJ (123 voxels) (see Materials and methods for more

Precuneus Seed fMRI

A Encoding Phase



B Distracter Phase



C Distracter vs. Encoding Phase

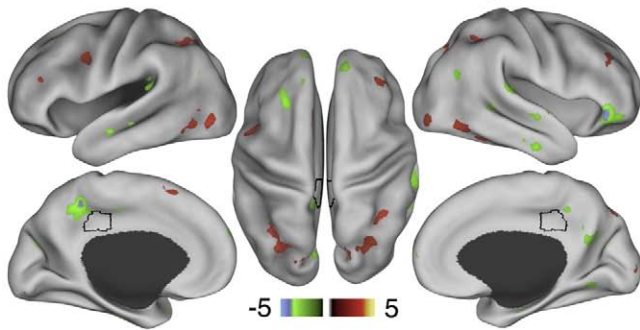


Fig. 7. Relationship between precuneus and default network at encoding and distracter phases. All maps are shown using Z statistics. Here we used an independent precuneus seed to demonstrate that: (A) During the encoding phase precuneus shows positive correlations (red-yellow colors) with the rest of the default network and negative correlations (green-blue colors) with the dorsal task network, analogous to the TPJ connectivity map at encoding. (B) During the distracter phase the pattern is largely similar. (C) Maps show results of a paired *t*-test comparing precuneus seed trial-based connectivity during distracter vs. encoding phase. Red-yellow maps shows regions where correlations with the precuneus seed increased from encoding to distracter phase, whereas the green-blue map shows regions where correlations with the precuneus seed decreased from encoding to distracter phase. As before, we show the map at $Z > 2.5$ threshold to indicate that, in contrast to TPJ, a canonical default system node does not show such “de-coupling,” also illustrated quantitatively for the entire DMN in Fig. 8. (For interpretation of the references to colour in this figure legend, the reader is referred to the web version of this article.)

573 details). The trial-based connectivity pattern at encoding for pre-
574 cuneus was quite similar to that found in the TPJ (Fig. 7A). However,
575 unlike TPJ, precuneus remained coupled with the rest of the DMN
576 during the distracter phase (Fig. 7B) and showed marked attenuation
577 of trial-based connectivity changes from encoding to distracter phase
578 (Fig. 7C). These results indicate that “de-coupling” with the DMN
579 during the distracter phase observed in the TPJ was not apparent
580 when examining a canonical DMN seed.

We confirmed the above results from the voxel-based analysis
581 using a ROI-based analysis that allowed us to explicitly compare TPJ
582 vs. DMN connectivity patterns and to use all DMN regions as ROIs, not
583 just the precuneus. Two questions were investigated: (1) Does TPJ
584 connectivity with explicitly defined DMN ROIs “weaken” from the
585 encoding phase to the distracter phase of WM?; (2) Does connectivity
586 within the DMN remain stable throughout the WM process? We
587 employed a ROI-based fMRI analysis using all 13 DMN nodes
588 explicitly defined based on the Fox and colleagues (2005) center of
589 mass coordinates that were the same size as the TPJ (see Materials and
590 methods). Correlations were computed between all ROI pairs for each
591 subject and then converted to Fisher Z values. The connections at
592 encoding and distracter phases were divided into: (1) DMN-to-DMN
593 correlations, reflecting only DMN pairs excluding TPJ and (2) TPJ-to-
594 DMN correlations reflecting all correlations between DMN nodes and
595 TPJ. Results shown in Fig. 8 indicate that DMN-to-DMN correlations
596 remained relatively stable at encoding and distracter phases;
597 however, TPJ-to-DMN ‘coupling’ weakened from encoding to dis-
598 tracter phase. To confirm this statistically, we computed a 2-way: *trial*
599 *phase* (encoding vs. distracter phase) \times *connection type* (DMN-to-
600 DMN connections vs. TPJ-to-DMN connections) repeated measures
601 ANOVA with subjects treated as the random factor. The ANOVA results
602 indicated a significant main effect of *phase* [$F(1,20) = 16.97$,
603 $p < 0.0006$], main effect of *connection type* [$F(1,20) = 5.1$, $p < 0.04$]
604 and a significant *trial phase* \times *connection type* interaction [$F(1,20)$
605 $= 15.75$, $p < 0.0008$]. The source of the interaction, as evident in Fig. 8,
606 was stable within-DMN coupling irrespective of trial phase, but
607 markedly weaker TPJ-to-DMN coupling at distracter phase. Taken
608 together, these results indicate that DMN-to-DMN coupling remains
609 stable throughout WM phases, whereas TPJ-to-DMN coupling weakens
610 as the WM process unfolds. 611

Discussion

The current study extends our understanding of TPJ function by
612 showing that: (1) TPJ suppression at encoding, prior to distracter
613 onset, predicts better WM performance and (2) the relationship
614 between TPJ and DMN regions changes over the course of the WM
615 process. DMN regions show greater suppression for correct vs.
616 incorrect trials during the encoding phase, similar to TPJ, but show
617 different activity patterns than TPJ during later phases of the trial.
618 Similarly, TPJ activity is coupled with DMN activity during the
619 encoding phase, but de-couples with the DMN during the distracter
620 phase. 621

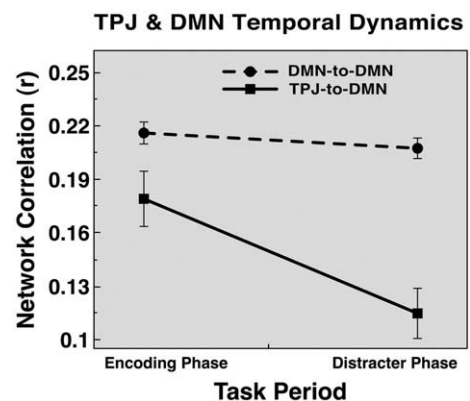


Fig. 8. TPJ and default network functional connectivity temporal dynamics. Seed-based pairwise correlations are shown averaged across all TPJ-to-DMN correlations (i.e. TPJ and each DMN node, solid line with squares) and all DMN-to-DMN correlations (i.e. each DMN node with every other DMN node, dotted line with circles). The correlations are shown at encoding and distracter phases. Overall, DMN-to-DMN connections remain stable across the WM phases, while TPJ-to-DMN functional connectivity “weakens” from encoding to distracter phase. Error bars represent ± 1 standard error of the mean.

622 phase, when it shows stronger correlations with nodes of the dorsal
623 attention network including dorsal frontal and parietal regions.

624 TPJ suppression during encoding

625 Previous models of TPJ function have proposed that TPJ is activated
626 in conjunction with dorsal fronto-parietal regions when attentional
627 re-allocation is needed (Corbetta et al., 2002). Given this function, TPJ
628 suppression may be needed when focused attention has to be
629 maintained, thus preventing reorienting to irrelevant objects (Shul-
630 man et al., 2007). While a version of the filter hypothesis was
631 formulated in the context of perceptual search (Shulman et al., 2003),
632 it has also been shown that TPJ is suppressed during WM function
633 (Todd et al., 2005). Here we showed that more TPJ suppression during
634 encoding was predictive of better WM performance within subjects.
635 The link between TPJ deactivation during encoding and WM
636 performance supports the filter hypothesis and suggests that TPJ
637 deactivation results in more efficient encoding of novel information
638 into WM. One possibility is that TPJ suppression during encoding
639 (along with suppression of other regions) may be necessary to dis-
640 engage operations (e.g. orienting) that can potentially disrupt optimal
641 WM trace formation. An important direction for future work will be to
642 more completely characterize TPJ response properties during WM
643 trace formation when encoding may be compromised via distraction.

644 TPJ function and working memory

645 The current results did not support the hypothesis that TPJ
646 deactivation, either during encoding or at later time points,
647 improves WM function by preventing subsequent TPJ activity to
648 non-target objects. The average TPJ activity to distracters was very
649 similar on correct and incorrect trials. While we cannot draw firm
650 conclusions regarding TPJ activity to non-target objects (see
651 below), one possibility is that—while TPJ activation is undesirable
652 during novel WM trace formation—once a strong WM trace is
653 achieved TPJ may be “freed up” to respond to incoming
654 behaviorally relevant information based on top-down signals
655 established during WM encoding (Corbetta et al., 2002, 2008;
656 Desimone and Duncan, 1995; Folk et al., 1992; Miller and Cohen,
657 2001; Posner et al., 1980; Treue, 2003). “Freeing up” orienting
658 responses during WM maintenance may allow flexible detection
659 and incorporation of additional environmental inputs in parallel
660 with WM maintenance, thus resulting in a more flexible behavioral
661 repertoire. Therefore, TPJ suppression may be critical while WM
662 traces are being formed and are still fragile (as demonstrated by
663 suppression results during encoding), but once the memory trace
664 has been robustly instantiated, elevated TPJ signals may not
665 provide an additional source of interference.

666 Alternatively, distracters in the current paradigm may not have
667 produced enough interference to warrant filtering via TPJ in the first
668 place. While overall performance during distraction was far from
669 perfect (79.6% correct, $N=40$), performance in the distraction-free
670 condition was lower (76.8% correct, $N=40$), stemming from the
671 surprisingly low accuracy in the distraction-free condition under high
672 WM load (68.6% correct, $N=40$). As noted earlier, while this is likely
673 an artifact of the present experimental design (i.e. mixing distracter
674 and distracter-free trials rather than blocking) it is still critical for
675 future work to demonstrate the absence of TPJ deactivation in
676 response to distracters even when such distraction results in worse
677 WM performance when compared to distracter-free trials. Similarly, it
678 will be important for future work to determine whether creating even
679 more interference—such as including multiple distracters—substan-
680 tially alters present findings, as it may be possible that TPJ responses
681 change substantially when multiple interfering stimuli are present.

682 In contrast to previous findings, we failed to observe a load-
683 dependent TPJ suppression (Todd et al., 2005). One possible reason

684 may be the strength of the present load manipulation. Our load
685 manipulation consisted of *three vs. two* memoranda items, with a
686 performance cost of 5.5% associated with the higher WM load
687 (ignoring the distracter-free condition). However, the manipulation
688 employed by Todd et al. (2005) consisted of *three vs. one* memoranda
689 item, with a performance cost of 11.34% associated with the higher
690 WM load. This discrepancy in difficulty between WM loads may have
691 produced the difference in load-dependent TPJ suppression. The
692 easier load manipulation in prior work resulted in near ceiling
693 performance (i.e. 94.13% correct), whereas the easier load manipula-
694 tion in the present study was virtually identical to the harder load
695 manipulation in prior work. In other words, our two-item memoranda
696 set may have produced near-maximal TPJ deactivation such that the
697 higher load added minimal further TPJ suppression resulting in the
698 absence of substantial load effects.

699 Lastly, some previous work focusing on subsequent memory
700 effects in WM (Pessoa et al., 2002) employed a blocked rather than
701 random presentation of distracters or trials (Sakai et al., 2002). One
702 possibility is that TPJ deactivation does not aid WM performance if the
703 nature of distraction is known a-priori (e.g. when distracter types are
704 blocked) as there may be other brain regions that mediate distracter
705 resistance in such instances (as shown by Sakai et al. 2002). It will be
706 important for future work to further characterize TPJ signals when
707 upcoming distraction is known vs. when it is not.

Default network suppression during encoding

709 A main finding was that a number of regions closely matching the
710 DMN also showed more suppression for correct vs. incorrect trials
711 during encoding, but not during later stages of WM. As with TPJ, these
712 results suggest that suppressing the DMN during formation of novel
713 memory traces may be critical for optimal WM operation. Considering
714 the proposed functions of the DMN (e.g. daydreaming, thinking about
715 one's future and past, broad internal information evaluation)
716 (Antrobus, 1991; Antrobus et al., 1970; Buckner and Carroll, 2007;
717 Mason et al., 2007; Mazoyer et al., 2001; Raichle et al., 2001; Raichle
718 and Snyder, 2007) deactivation of the DMN may be critical at times of
719 sustained cognitive engagement with the environment and especially
720 during formation of memory representations. Also, given the putative
721 importance of temporarily “deactivating” the TPJ to achieve atten-
722 tional filtering, TPJ and DMN regions may become coupled when their
723 temporary disengagement is imperative, thus ensuring robust WM
724 trace formation.

Relationship between TPJ and the default network

726 TPJ was coupled with DMN regions during encoding of
727 information into WM, although this coupling is not observed in
728 the resting state (Fox et al., 2005; He et al., 2007). Interestingly,
729 this pattern of trial-based connectivity with the DMN changed as
730 the WM process unfolded, with less connectivity during the
731 distracter phase. The opposite pattern of connectivity was observed
732 between the TPJ and components of the dorsal attention system (as
733 well as MFG and other frontal and anterior insula regions)
734 supporting the hypothesis that TPJ signals reflect an “orienting”
735 function separate from the function of the DMN. Thus, TPJ may
736 interact with the dorsal attention system as novel task-relevant
737 information emerges in the external environment and needs to be
738 evaluated in parallel while WM traces are actively maintained
739 (Corbetta et al., 2008). Consistent with these different functional
740 roles of TPJ and DMN, TPJ showed greater responsiveness than
741 DMN specifically to distracters sharing features with the current
742 task (Serences et al., 2005). In summary, the fMRI findings suggest
743 that the TPJ may not be functionally static, but instead may
744 dynamically connect with different networks depending on
745 ongoing task demands.

746 Limitations and future directions

747 One of the main limitations of this study is the correlational nature
748 of fMRI data and behavior. It will be important for future work to
749 confirm present findings by employing methods that could establish
750 more direct causal links between TPJ function and behavior (e.g.
751 TMS). Furthermore, given the relatively slow time resolution of fMRI it
752 is at present unknown precisely when de-coupling from the DMN
753 nodes may occur. To better understand the precise temporal pattern
754 of TPJ and the DMN interaction the use of other converging non-
755 invasive techniques with more precise timing will be important (e.g.
756 MEG and EEG). One important consideration for future studies of TPJ
757 function, both in the context of attentional processes and other
758 putative TPJ functions (e.g. theory of mind studies), is that TPJ
759 dynamics may be time sensitive both in terms of activation patterns
760 and pattern of connectivity with other brain regions. These dynamics
761 may depend on changing task demands and this consideration
762 becomes particularly important when interpreting TPJ function in
763 the context of experiments using blocked designs, which average
764 activity over possibly diverse processes.

765 Conclusion

766 The current study extended our understanding of TPJ function by
767 demonstrating the functional significance of TPJ and DMN suppression
768 when WM traces are still forming. Additionally, we presented
769 evidence that TPJ strongly couples with the DMN during encoding, but
770 dissociates from the DMN both in terms of task-evoked signals and
771 functional connectivity during later WM stages. An important venue
772 for future research will be to better characterize TPJ dynamics during
773 WM trace formation in the presence of distraction as well as the
774 functional importance of changing connectivity between TPJ and
775 other brain regions.

776 Acknowledgments

777 We thank T. Braver for helpful comments and analysis suggestions.
778 We also thank M. Fox for allowing us to use previously published data
779 to verify our findings. Supported by NIMH grant MH06603101 (DMB)
780 funded by the National Institute of Mental Health.

781 Appendix A. Supplementary data

782 Supplementary data associated with this article can be found in,
783 the online version, at doi:10.1016/j.neuroimage.2009.11.008.

784 References

- 785 Antrobus, J., 1991. Dreaming: cognitive processes during cortical activation and high
786 afferent thresholds. *Psychol. Rev.* 98, 96–121.
787 Antrobus, J.S., Singer, J.L., Goldstein, S., Fortgang, M., 1970. Mindwandering and
788 cognitive structure. *Trans. N. Y. Acad. Sci.* 32, 242–252.
789 Arrington, C.M., Carr, T.H., Mayer, A.R., Rao, S.M., 2000. Neural mechanisms of visual
790 attention: object-based selection of a region in space. *J. Cogn. Neurosci.*
791 Attneave, F., Arnoult, M.D., 1956. The quantitative study of shape and pattern
792 perception. *Psychol. Bull.* 53, 452–471.
793 Boynton, G.M., Engel, S.A., Glover, G.H., Heeger, D.J., 1996. Linear systems analysis of
794 functional magnetic resonance imaging in human V1. *J. Neurosci.* 16, 4207–4221.
795 Bradley, M.M., Hamby, S., Löw, A., Lang, P.J., 2007. Brain potentials in perception:
796 picture complexity and emotional arousal. *Psychophysiology* 44, 364–373.
797 Buckner, R.L., Carroll, D.C., 2007. Self-projection and the brain. *Trends Cogn. Sci. (Regul.*
798 *Ed.)* 11, 49–57.
799 Buckner, R.L., Head, D., Parker, J., Fotenos, A.F., Marcus, D., Morris, J.C., Snyder, A.Z., 2004.
800 A unified approach for morphometric and functional data analysis in young, old,
801 and demented adults using automated atlas-based head size normalization:
802 reliability and validation against manual measurement of total intracranial volume.
803 *NeuroImage* 23, 724–738.
804 Buckner, R.L., Snyder, A.Z., Shannon, B.J., LaRossa, G., Sachs, R., Fotenos, A.F., Sheline, Y.L.,
805 Klunk, W.E., Mathis, C.A., Morris, J.C., Mintun, M.A., 2005. Molecular, structural, and
806 functional characterization of Alzheimer's disease: evidence for a relationship
807 between default activity, amyloid, and memory. *J. Neurosci.* 25, 7709–7717.

- Collin, C.A., McMullen, P.A., 2002. Using Matlab to generate families of similar Attneave
808 shapes. *Behavior Research Methods, Instruments, & Computers: a Journal of the*
809 *Psychonomic Society, Inc* 34, 55–68.
810 Corbetta, M., Kincade, J.M., Shulman, G.L., 2002. Neural systems for visual orienting and
811 their relationships to spatial working memory. *J. Cogn. Neurosci.* 14, 508–523.
812 Corbetta, M., Kincade, M.J., Ollinger, J.M., McAvoy, M.P., Shulman, G.L., 2000. Voluntary
813 orienting is dissociated from target detection in human posterior parietal cortex.
814 *Nat. Neurosci.* 3, 292–297.
815 Corbetta, M., Patel, G., Shulman, G.L., 2008. The reorienting system of the human brain:
816 from environment to theory of mind. *Neuron* 58, 306–324.
817 Delplanque, S., N'diaye, K., Scherer, K., Grandjean, D., 2007. Spatial frequencies or
818 emotional effects? A systematic measure of spatial frequencies for IAPS pictures by
819 a discrete wavelet analysis. *J. Neurosci. Methods* 165, 144–150.
820 Desimone, R., Duncan, J., 1995. Neural mechanisms of selective visual attention. *Annu.*
821 *Rev. Neurosci.* 18, 193–222.
822 Dolcos, F., McCarthy, G., 2006. Brain systems mediating cognitive interference by
823 emotional distraction. *J. Neurosci.* 26, 2072–2079.
824 Dolcos, F., Diaz-Granados, P., Wang, L., McCarthy, G., 2008. Opposing influences of
825 emotional and non-emotional distracters upon sustained prefrontal cortex activity
826 during a delayed-response working memory task. *Neuropsychologia* 46, 326–335.
827 Downar, J., Crawley, A.P., Mikulis, D.J., Davis, K.D., 2000. A multimodal cortical network
828 for the detection of changes in the sensory environment. *Nat. Neurosci.* 3, 277–283.
829 Downar, J., Crawley, A.P., Mikulis, D.J., Davis, K.D., 2001. The effect of task relevance on
830 the cortical response to changes in visual and auditory stimuli: an event-related
831 fMRI study. *NeuroImage* 6, 1256–1267.
832 Downar, J., Crawley, A.P., Mikulis, D.J., Davis, K.D., 2002. A cortical network sensitive to
833 stimulus salience in a neutral behavioral context across multiple sensory
834 modalities. *J. Neurophysiol.* 87, 615–620.
835 Folk, C.L., Remington, R.W., Johnston, J.C., 1992. Involuntary covert orienting is
836 contingent on attentional control settings. *J. Exp. Psychol. Hum. Percept. Perform.*
837 18, 1030–1044.
838 Fox, M.D., Snyder, A.Z., Vincent, J.L., Corbetta, M., Van Essen, D.C., Raichle, M.E., 2005.
839 The human brain is intrinsically organized into dynamic, anticorrelated functional
840 networks. *Proc. Natl. Acad. Sci. U. S. A.* 102, 9673–9678.
841 Fox, M.D., Corbetta, M., Snyder, A.Z., Vincent, J.L., Raichle, M.E., 2006. Spontaneous
842 neuronal activity distinguishes human dorsal and ventral attention systems. *Proc.*
843 *Natl. Acad. Sci. U. S. A.* 103, 10046–10051.
844 Greicius, M.D., Krasnow, B., Reiss, A.L., Menon, V., 2003. Functional connectivity in the
845 resting brain: a network analysis of the default mode hypothesis. *Proc. Natl. Acad.*
846 *Sci. U. S. A.* 100, 253–258.
847 Hampson, M., Driesen, N.R., Skudlarski, P., Gore, J.C., Constable, R.T., 2006. Brain
848 connectivity related to working memory performance. *J. Neurosci.* 26,
849 13338–13343.
850 He, B.J., Snyder, A.Z., Vincent, J.L., Epstein, A., Shulman, G.L., Corbetta, M., 2007.
851 Breakdown of functional connectivity in frontoparietal networks underlies
852 behavioral deficits in spatial neglect. *Neuron* 53, 905–918.
853 Indovina, I., Macaluso, E., 2007. Dissociation of stimulus relevance and saliency factors
854 during shifts of visuospatial attention. *Cereb. Cortex* 17, 1701–1711.
855 Kerr, D.L., Gusnard, D.A., Snyder, A.Z., Raichle, M.E., 2004. Effect of practice on reading
856 performance and brain function. *NeuroReport* 15, 607–610.
857 Kincade, J.M., Abrams, R.A., Astafiev, S.V., Shulman, G.L., Corbetta, M., 2005. An event-
858 related functional magnetic resonance imaging study of voluntary and stimulus-
859 driven orienting of attention. *J. Neurosci.* 25, 4593.
860 Lang, P.J., Bradley, M.M., Cuthbert, B.N., 1999. International affective picture system
861 (IAPS): Technical manual and affective ratings. University of Florida, Gainesville.
862 Macaluso, E., Frith, C.D., Driver, J., 2002. Directing attention to locations and to sensory
863 modalities: multiple levels of selective processing revealed with PET. *Cereb. Cortex*
864 12, 357–368.
865 Marois, R., Leung, H.C., Gore, J., 2000. A stimulus-driven approach to object identity and
866 location processing in the human brain. *Neuron*.
867 Mason, M.F., Norton, M.I., Van Horn, J.D., Wegner, D.M., Grafton, S.T., Macrae, C.N., 2007.
868 Wandering minds: the default network and stimulus-independent thought. *Science*
869 315, 393–395.
870 Mazoyer, B., Zago, L., Mellet, E., Bricogne, S., Etard, O., Houdé, O., Crivello, F., Joliot, M.,
871 Petit, L., Tzourio-Mazoyer, N., 2001. Cortical networks for working memory and
872 executive functions sustain the conscious resting state in man. *Brain Res. Bull.* 54,
873 287–298.
874 McKiernan, K.A., Kaufman, J.N., Kucera-Thompson, J., Binder, J.R., 2003. A parametric
875 manipulation of factors affecting task-induced deactivation in functional neuroimaging.
876 *J. Cogn. Neurosci.* 15, 394–408.
877 Michelon, P., Snyder, A.Z., Buckner, R.L., McAvoy, M., Zacks, J.M., 2003. Neural correlates
878 of incongruous visual information. An event-related fMRI study. *NeuroImage* 19,
879 1612–1626.
880 Miller, E.K., Cohen, J.D., 2001. An integrative theory of prefrontal cortex function. *Annu.*
881 *Rev. Neurosci.* 21, 167–202.
882 Ojemann, J., Akbudak, E., Snyder, A., McKinstry, R., Raichle, M., Conturo, T., 1997.
883 Anatomic localization and quantitative analysis of gradient refocused echo-planar
884 fMRI susceptibility artifacts. *NeuroImage* 6, 156–167.
885 Pessoa, L., Gutierrez, E., Bandettini, P., Ungerleider, L., 2002. Neural correlates of visual
886 working memory: fMRI amplitude predicts task performance. *Neuron* 35,
887 975–987.
888 Posner, M.I., Snyder, C.R., Davidson, B.J., 1980. Attention and the detection of signals.
889 *J. Exp. Psychol.* 109, 160–174.
890 Raichle, M.E., MacLeod, A.M., Snyder, A.Z., Powers, W.J., Gusnard, D.A., Shulman, G.L.,
891 2001. A default mode of brain function. *Proc. Natl. Acad. Sci. U. S. A.* 98,
892 676–682.
893

- 894 Ralchle, M.E., Snyder, A.Z., 2007. A default mode of brain function: a brief history of an
895 evolving idea. *NeuroImage* 37, 1083–1090.
- 896 Sabatinelli, D., Bradley, M.M., Fitzsimmons, J.R., Lang, P.J., 2005. Parallel amygdala
897 and inferotemporal activation reflect emotional intensity and fear relevance.
898 *NeuroImage* 24, 1265–1270.
- 899 Sakai, K., Rowe, J.B., Passingham, R.E., 2002. Active maintenance in prefrontal area 46
900 creates distractor-resistant memory. *Nat. Neurosci.* 5, 479–484.
- 901 Serences, J.T., Shomstein, S., Leber, A.B., Golay, X., 2005. Coordination of voluntary
902 and stimulus-driven attentional control in human cortex. *Psychol. Sci.* 16,
903 114–122.
- 904 Shulman, G.L., Fiez, J.A., Corbetta, M., Buckner, R.L., Miezin, F.M., Raichle, M.E., Peterson,
905 S.E., 1997. Common blood flow changes across visual tasks: II. decreases in cerebral
906 cortex. *J. Cogn. Neurosci.* 9, 648–663.
- 907 Shulman, G.L., McAvoy, M.P., Cowan, M.C., Astafiev, S.V., Tansy, A.P., d'Avossa, G.,
908 Corbetta, M., 2003. Quantitative analysis of attention and detection signals during
909 visual search. *J. Neurophysiol.* 90, 3384–3397.
- 910 Shulman, G.L., Astafiev, S.V., McAvoy, M.P., d'Avossa, G., Corbetta, M., 2007. Right TPJ
911 deactivation during visual search: functional significance and support for a filter
912 hypothesis. *Cereb. Cortex* 17, 2625–2633.
- 913 Sternberg, S., 1969. The discovery of processing stages: Extensions of Donders' method.
914 In: Koster, W.G. (Ed.), *Attention and performance II*. North-Holland, Amsterdam.
- 915 Talairach, J., Tournoux, P., 1988. *Co-planar stereotaxic atlas of the human brain*. Thieme,
916 New York.
- 917 Todd, J.J., Fougny, D., Marois, R., 2005. Visual short-term memory load suppresses
918 temporo-parietal junction activity and induces inattentive blindness. *Psychol.*
919 *Sci.* 16, 965–972.
- 920 Treue, S., 2003. Visual attention: the where, what, how and why of saliency. *Curr. Opin.*
921 *Neurobiol.* 13, 428–432.
- 922 Van Essen, D.C., 2005. A Population-Average, Landmark- and Surface-based (PALS) atlas
923 of human cerebral cortex. *NeuroImage* 28, 635–662.
- 924 Worsley, K.J., Friston, K.J., 1995. Analysis of fMRI time-series revisited—again.
925 *NeuroImage* 2, 173–181.

UNCORRECTED PROOF